

**SIMULATION OF UNDERFILL  
ENCAPSULATION OF  
ELECTRONIC PACKAGING USING  
THE LATTICE-BOLTZMANN METHOD**

**GAN ZHONG LI**

**UNIVERSITI SAINS MALAYSIA**

**2018**

**SIMULATION OF UNDERFILL ENCAPSULATION OF  
ELECTRONIC PACKAGING USING  
THE LATTICE-BOLTZMANN METHOD**

**by**

**GAN ZHONG LI**

**Thesis submitted in fulfilment of the  
requirements for the Degree of  
Master of Science**

**April 2018**

## **ACKNOWLEDGEMENT**

First and foremost, I would like to express my sincere gratitude to my supervisor, Dr. Aizat Abas for his guidance, advices, commitment and the financial support throughout the course of my master's degree. I would not be able to finish the project within the allocated time frame without his dedication in steering this effort in the right direction.

I would also like to thank my fellow comrades, Ng Fei Chong, Norhafizah and Siti Haslinda, who were under Dr. Aizat's supervision as well, for all the assistance and suggestions I received throughout my studies.

The Ministry of Higher Education has always been supportive towards students who wished to further their studies. I hereby would like to thank the MyBrain15 scholarship I have received during my course of study. The financial aid given had definitely eased my financial burden in paying my tuition fees. I would like to thank the FRGS grant which has funded my research program.

On the personal side, I would like to thank my parents for their understanding and unconditional support given throughout my studies. I could not have done it without the emotional and mental given by them. Thank you for being there with me during tough times. I could not have successfully finish my dissertation without them.

I would also like to thank my beloved friends for all the support I have received. Their constant support and companionship have encouraged me to overcome the odds and face every challenges with perseverance and bravery.

Lastly, a big shout out to everyone who had supported me, either directly or indirectly, along my way in finishing this dissertation.

## TABLE OF CONTENTS

	<b>Page</b>
<b>ACKNOWLEDGEMENT</b>	ii
<b>TABLE OF CONTENTS</b>	iii
<b>LIST OF TABLES</b>	vii
<b>LIST OF FIGURES</b>	ix
<b>LIST OF PLATES</b>	xvi
<b>LIST OF SYMBOLS</b>	xvii
<b>LIST OF ABBREVIATIONS</b>	xviii
<b>ABSTRAK</b>	xix
<b>ABSTRACT</b>	xxi
<b>CHAPTER ONE: INTRODUCTION</b>	
1.1 Introduction	1
1.1.1 Underfill encapsulation process	3
1.1.2 Lattice-Boltzmann method	5
1.1.3 Particle image velocimetry	6
1.2 Project background	7
1.3 Problem statement	8
1.4 Objectives	10
1.5 Contribution of the study	10
1.6 Scope of study	11
1.7 Thesis outline	12
<b>CHAPTER TWO: LITERATURE REVIEW</b>	
2.1 Introduction	13
2.2 Lattice-Boltzmann method	14
2.3 Volume of Fluid	17
2.4 Mass Loss	18
2.5 Knudsen Number	19
2.6 Underfill encapsulation	20
2.7 Effects of solder joint geometry on component reliability	27
2.8 Particle image velocimetry	31

2.9	Summary	34
-----	---------	----

### **CHAPTER THREE: METHODOLOGY**

3.1	Governing Equations	37
3.1.1	Lattice-Boltzmann formulation	37
3.1.2	LBM Volume of fluid-free surface formulations	40
3.1.3	Boundary condition: bounce-back formulation	42
3.2	Numerical simulation	43
3.2.1	Bond number	45
3.2.2	Knudsen number	46
3.2.3	Boundary conditions	46
3.2.4	Convergence study	47
3.2.5	Simulation mass loss	48
3.3	Geometry set up	49
3.3.1	Effects of different solder joint arrangements on underfill encapsulation process	49
3.3.2	Effects of different injection methods on capillary underfill process	50
3.3.3	Effects of different solder joint shapes on U-type dispensing capillary underfill	51
3.3.4	Comparison between capillary and pressurised underfill	52
3.4	Experimental study	53
3.4.1	Conventional experiment study	53
3.4.2	PIV experiment	55
3.5	PIV Analysis	58
3.5.1	Image pre-processing	59
3.5.2	Image evaluation	60
3.5.3	Post-processing	62

### **CHAPTER FOUR: RESULTS AND DISCUSSIONS**

4.1	Effects of different solder joint arrangements on underfill encapsulation process	63
4.1.1	Filling time	64
4.1.2	Flow front comparison	66
4.1.3	Velocity distribution of flow	71

4.1.4	Pressure distribution of flow	78
4.1.5	Formation of void	80
4.1.6	Summary	82
4.2	Effects of different injection method on capillary underfill process	83
4.2.1	Filling time	83
4.2.2	Flow front comparison	87
4.2.3	Velocity distribution of flow	91
4.2.4	Pressure distribution of flow	96
4.2.5	Void formation	99
4.2.6	Summary	101
4.3	Effects of different solder joint shapes on U-type dispensing capillary underfill	102
4.3.1	Filling time	102
4.3.2	Flow front comparison	105
4.3.3	Velocity distribution of flow	109
4.3.4	Pressure distribution of flow	116
4.3.5	Formation of void	118
4.3.6	Effects of different hourglass shape of similar aspect ratio and shape ratio on underfill flow	121
4.3.7	Summary	127
4.4	Comparison between capillary underfill and pressurised underfill	128
4.4.1	Filling time	128
4.4.2	Flow front comparison	133
4.4.3	Formation of void	139
4.4.4	Velocity distribution of flow	142
4.4.5	Pressure distribution of flow	146
4.4.6	Summary	152

## **CHAPTER FIVE: CONCLUSIONS**

5.1	Conclusions	153
5.2	Recommendations for future works	155

<b>REFERENCES</b>	157
-------------------	-----

## **APPENDICES**

- Appendix A: Setting Up Cygwin on Windows
- Appendix B: Compilation and Execution of Palabos within Cygwin
- Appendix C: Sample simulation code
- Appendix D: Vector field of underfill flow with different BGA arrangement
- Appendix E: Velocity contour with vector overlay of underfill flow with different BGA arrangement
- Appendix F: Vector field of underfill flow with different injection methods
- Appendix G: Velocity contour with vector overlay of underfill flow with different BGA arrangement
- Appendix H: Vector field of underfill flow of BGA with different solder joint shapes
- Appendix I: Velocity contour with vector overlay of underfill flow of BGA with different solder joint shapes

## **LIST OF PUBLICATIONS**

## LIST OF TABLES

		<b>Page</b>
Table 3.1	Weighting functions for a D3Q19 model	39
Table 3.2	Cell types together with its distribution function, volume fraction and possible transformation	41
Table 3.3	Material properties of underfill encapsulant material	44
Table 3.4	Comparison of density and viscosity of industrial-use underfill materials with experimental underfill materials.	45
Table 3.5	Resolution of lattice model with the corresponding number of lattice, pressure values and discretisation error	47
Table 3.6	Solder joints' dimensions, aspect ratio and shape factor	51
Table 4.1	Underfill filling time for I-type dispensing of solder joint array of different arrangements	64
Table 4.2	Filling time and percentage difference between simulation and experimental filling time for solder joint array of different arrangements	65
Table 4.3	Comparison of velocity values and its percentage differences probed at location A for different solder joint arrangements at different filling percentage	76
Table 4.4	Underfill filling time for different injection methods at different filling percentages	84
Table 4.5	Comparison of simulation and experimental filling time with error bar for different injection methods	86
Table 4.6	Comparison of velocity values and its percentage differences probed at location A for different injection methods at different filling percentages	95
Table 4.7	Underfill filling time for BGA of different solder joint shapes at different filling percentage	102
Table 4.8	Percentage difference between simulation and experimental filling time	104
Table 4.9	Comparison of velocity values and its percentage differences probed at location A for different solder joint shapes at different filling percentages	114

Table 4.10	Comparison of velocity values and its percentage differences probed at location B for different solder joint shapes at different filling percentages	114
Table 4.11	Filling time comparison between different hour glass shaped solder joint	122
Table 4.12	Velocity at probed location at various filling percentages	126
Table 4.13	Filling time at different filling percentage for capillary and pressurised underfill	128
Table 4.14	Percentage of reduction of filling time for pressurised underfill for different inlet pressure relative to capillary underfill	130
Table 4.15	Percentage of reduction of filling time for pressurised underfill for different inlet pressure	131
Table 4.16	Percentage difference between simulation and experimental filling time for capillary and pressurised underfill	144
Table 4.17	Velocity values at probed location at different filling percentages for different inlet configurations	144

## LIST OF FIGURES

		<b>Page</b>
Figure 1.1	Electronic Packaging Hierarchy	2
Figure 1.2	Arrangement of solder balls underneath Intel Embedded Pentium MMX processor	3
Figure 1.3	Capillary underfill process of BGA package	4
Figure 1.4	Pressurised underfill setup	5
Figure 1.5	General PIV setup	6
Figure 2.1	Velocities along links cutting the boundary surface as indicated by the arrows. Boundary nodes are represented by open squares, while the fluid nodes are represented by solid circles (Nguyen and Ladd, 2002).	18
Figure 2.2	Micro-PIV setup for underfill flow study	33
Figure 3.1	D3Q19 lattice model	37
Figure 3.2	A 2D representation of liquid-air interface (The dash line represents the real interface)	40
Figure 3.3	Half-way bounce-back scheme on D2Q9 lattice model	42
Figure 3.4	Boundary conditions setup for bounce back and periodic conditions (① - Periodic boundary conditions, ② - Wall boundary conditions)	47
Figure 3.5	Graph of pressure value against number of lattice	48
Figure 3.6	Solder joint arrangements	49
Figure 3.7	Dimension of BGA setup (for study of different solder joint arrangements)	50
Figure 3.8	Dimension and arrangement of BGA setup (for study of different injection methods)	50
Figure 3.9	Schematic drawing of the side view of different solder joint shapes	51
Figure 3.10	Dimension and arrangement of the BGA setup (for study of different solder joint shapes)	52
Figure 3.11	Dimension and arrangement of the BGA setup (for study of comparison between capillary and pressurised underfill)	53

Figure 3.12	Schematic view of capillary underfill setup	54
Figure 3.13	Schematic view of pressurised underfill setup	54
Figure 3.14	Schematic diagram of PIV experimental setup	57
Figure 3.15	Workflow of the digital PIV analysis	58
Figure 3.16	Figures that are obtained after the corresponding image pre-processing steps	60
Figure 3.17	Masks (shaded in red) applied onto PIV image	61
Figure 4.1	WLCSP package (“PCB Layout Recommendations for BGA Packages,” 2017) vs simulation model	63
Figure 4.2	Comparison of filling time for I-type dispensing of solder joint array of different arrangement	64
Figure 4.3	Comparison of simulation and experimental filling time with error bar for solder joint array of different arrangements	66
Figure 4.4	Comparison of flow front at different filling percentages between simulation and experiment underfill flow for full array BGA	67
Figure 4.5	Comparison of flow front at different filling percentages between simulation and experiment underfill flow for middle empty BGA arrangement	68
Figure 4.6	Comparison of flow front at different filling percentages between simulation and experiment underfill flow for perimeter BGA arrangement	69
Figure 4.7	Comparison of velocity contour at different filling percentages between simulation and experiment underfill flow for full array BGA arrangement	71
Figure 4.8	Comparison of velocity contour at different filling percentages between simulation and experiment underfill flow for middle empty BGA arrangement	72
Figure 4.9	Comparison of velocity contour at different filling percentages between simulation and experiment underfill flow for perimeter BGA arrangement	73
Figure 4.10	Location of probe (for study of different solder joint arrangements)	76

Figure 4.11	Comparison of velocity values at point A between different solder joint arrangements for both simulation and experimental results	77
Figure 4.12	Comparison of pressure contours during capillary underfill of BGA with different solder joint arrangements (all units in Pa)	78
Figure 4.13	Graph of pressure against time at Point A for underfill of BGA with different solder joint arrangements	79
Figure 4.14	Formation of void for different BGA arrangement	81
Figure 4.15	Mechanism of void formation due to viscous fingering	81
Figure 4.16	I-type, L-type and U-type injection methods	83
Figure 4.17	Comparison of filling time for different injection methods for both simulation and experimental results	84
Figure 4.18	Comparison of simulation and experimental filling time with error bar for different injection methods.	86
Figure 4.19	Comparison of flow front at different filling percentages between simulation and experiment underfill flow for I-type injection method	88
Figure 4.20	Comparison of flow front at different filling percentages between simulation and experiment underfill flow for L-type injection method	89
Figure 4.21	Comparison of flow front at different filling percentages between simulation and experiment underfill flow for U-type injection method	90
Figure 4.22	Comparison of velocity contour at different filling percentages between simulation and experiment underfill flow for I-type injection method	91
Figure 4.23	Comparison of velocity contour at different filling percentages between simulation and experiment underfill flow for L-type injection method	92
Figure 4.24	Comparison of velocity contour at different filling percentages between simulation and experiment underfill flow for U-type injection method	93
Figure 4.25	Location of probe “A” (for study of different injection methods)	94

Figure 4.26	Comparison of velocity values at point A between different injection methods for both simulation and experimental results	95
Figure 4.27	Comparison of pressure contours during capillary underfill of BGA with different injection methods (all units in Pa)	97
Figure 4.28	Graph of pressure against time at Point A for underfill of BGA with different injection methods	98
Figure 4.29	Comparison of flow front for different injection methods at near completion of filling	100
Figure 4.30	Formation of void in U-type injection method due to racing effect	101
Figure 4.31	Comparison of filling time between different solder joint shapes for both simulation and experimental results	103
Figure 4.32	Comparison of simulation and experimental filling time with error bar for BGA with different solder joint shapes	104
Figure 4.33	Comparison of flow front at different filling percentages between simulation and experiment underfill flow for truncated spherical shaped solder joints	105
Figure 4.34	Comparison of flow front at different filling percentages between simulation and experiment underfill flow for cylindrical shaped solder joints	106
Figure 4.35	Comparison of flow front at different filling percentages between simulation and experiment underfill flow for hourglass shaped solder joints	107
Figure 4.36	Perspective distortion on hourglass shape solder joint	109
Figure 4.37	Comparison of velocity contour at different filling percentages between simulation and experiment underfill flow for truncated spherical shaped solder joints	110
Figure 4.38	Comparison of velocity contour at different filling percentages between simulation and experiment underfill flow for cylindrical shaped solder joints	111
Figure 4.39	Comparison of velocity contour at different filling percentages between simulation and experiment underfill flow for hourglass shaped solder joints	112
Figure 4.40	Location of probe (for study of different solder joint shapes)	113

Figure 4.41	Comparison of velocity values at point A between different solder joint shapes for both simulation and experimental results	115
Figure 4.42	Comparison of velocity values at point B between different solder joint shapes for both simulation and experimental results	116
Figure 4.43	Comparison of pressure contours during underfill of BGA of different solder joint shapes (all units in Pa)	117
Figure 4.44	Graph of pressure against time at point B for BGA with different solder joint shapes	118
Figure 4.45	Comparison of flow front moments after coalescing of flow fronts approaching from two opposite directions	119
Figure 4.46	Different hourglass shaped solder joint of similar aspect ratios and shape factor (Left - Two conjoined hemispheres. Right – Parabolic curve sides)	121
Figure 4.47	Filling time comparison between different hour glass shaped solder joint	122
Figure 4.48	Comparison of underfill flow front at different filling percentages for different hourglass shaped solder joints	124
Figure 4.49	Cross sectional plane	125
Figure 4.50	Velocity profile of cross sections for underfill flow across different BGA shapes at different filling percentages (all units in m/s)	125
Figure 4.51	Probed location (marked by white colour + symbol) on cross section	126
Figure 4.52	Velocity at probed location at various filling percentages	126
Figure 4.53	Comparison of filling time between simulation and experimental results for capillary underfill	129
Figure 4.54	Comparison of filling time between simulation and experimental results for pressurised underfill at different inlet pressure	129
Figure 4.55	Time taken for complete filling against pressurised underfill inlet pressure	131
Figure 4.56	Comparison of simulation and experimental filling time with error bar for capillary underfill	133

Figure 4.57	Comparison of simulation and experimental filling time with error bar for pressurised underfill	133
Figure 4.58	Comparison between simulation and experiment flow front (capillary underfill)	134
Figure 4.59	Comparison between simulation and experiment flow front (pressurised underfill – 689.48kPa)	135
Figure 4.60	Comparison between simulation and experiment flow front (pressurised underfill – 1378.98kPa)	136
Figure 4.61	Comparison between simulation and experiment flow front (pressurised underfill – 2068.43kPa)	137
Figure 4.62	Comparison between simulation and experiment flow front (pressurised underfill – 2757.90kPa)	138
Figure 4.63	Void formation at the experimental results (as indicated by the arrows) at 689.48kPa at 80% of flow	140
Figure 4.64	Simulated underfill flow at 60% filling	140
Figure 4.65	Velocity distribution of fluid flow at various filling percentage (capillary underfill, all units in mm/s)	142
Figure 4.66	Velocity distribution of fluid flow at various filling percentage (pressurised underfill – 689.48kPa, all units in mm/s)	142
Figure 4.67	Velocity distribution of fluid flow at various filling percentage (pressurised underfill – 1378.95kPa, all units in mm/s)	142
Figure 4.68	Velocity distribution of fluid flow at various filling percentage (pressurised underfill – 2068.43kPa, all units in mm/s)	143
Figure 4.69	Velocity distribution of fluid flow at various filling percentage (pressurised underfill – 2757.90kPa, all units in mm/s)	143
Figure 4.70	Location of probe (for study of comparison between capillary and pressurised underfill)	144
Figure 4.71	Graph of velocity against filling percentage at probed location for capillary underfill	145
Figure 4.72	Graph of velocity against filling percentage at probed location for pressurised underfill	145

Figure 4.73	Pressure distribution of fluid flow at various filling percentage (capillary underfill, all units in kPa)	146
Figure 4.74	Pressure distribution of fluid flow at various filling percentage (pressurised underfill – 689.48kPa, all units in kPa)	147
Figure 4.75	Pressure distribution of fluid flow at various filling percentage (pressurised underfill – 1378.95kPa, all units in kPa)	147
Figure 4.76	Pressure distribution of fluid flow at various filling percentage (pressurised underfill – 2068.43kPa, all units in kPa)	147
Figure 4.77	Pressure distribution of fluid flow at various filling percentage (pressurised underfill – 2757.90kPa, all units in kPa)	148
Figure 4.78	Graph of pressure against time at point A for capillary underfill	149
Figure 4.79	Graph of pressure against time at point A for pressurised underfill	150
Figure 4.80	Peak pressure vs inlet pressure	151
Figure 4.81	Fluid pressure acting against the PCB	151

## LIST OF PLATES

		<b>Page</b>
Plate 3.1	Actual solder joints of different shapes used in experiment	51
Plate 3.2	(Left) Pressurised underfill setup (Right) Top view of BGA in pressurised underfill setup	54
Plate 3.3	PIV experimental setup on top of a light box	57

## LIST OF SYMBOLS

$\epsilon$	Volume fraction
$\rho$	Density
$\sigma$	Standard deviation
$\tau$	Relaxation factor
$\Omega$	Collision operator
$\omega$	Collision frequency
$\mathbf{e}$	Microscopic velocity
$A$	Interrogation matrix
$B$	Interrogation matrix
$C$	Cross-correlation function
$L$	Reference length
$M$	Mass content
$c$	Basic speed of lattice
$f$	Single particle distribution equation
$i$	Coordinate in horizontal axis
$j$	Coordinate in vertical axis
$t$	Time
$u$	Velocity
$w$	Weight
$x$	Position

## LIST OF ABBREVIATIONS

BGA	Ball Grid Array
BGK	Bhatnagar-Groos-Krook
CFD	Computational Fluid Dynamics
DCC	Direct Cross Correlation
DFT	Discrete Fourier Transform
DPIV	Digital Particle Image Velocimetry
EMC	Epoxy Moulded Compound
FE	Finite Element
FEM	Finite Element Method
FVM	Finite Volume Method
IC	Integrated Circuit
IDE	Integrated Development Environment
LBM	Lattice-Boltzmann Method
LED	Light Emitting Diode
MPI	Message Passing Interface
N-S	Navier-Stokes
PCB	Printed Circuit Board
PIV	Particle Image Velocimetry
SMT	Surface Mount Technology
SPH	Smoothed Particle Hydrodynamics
TSV	Through-Silicon Via
VOF	Volume of Fluid

# **SIMULASI PENGKAPSULAN ISIAN BAWAH PAKEJ ELEKTRONIK MENGUNAKAN KAEDAH KEKISI BOLTZMANN**

## **ABSTRAK**

Kebanyak kajian berasaskan kaedah isipadu terhingga (FVM) telah dilaksanakan untuk mengoptimumkan dan memperbaiki proses pengkapsulan isian bawah. Namun, terdapat kajian yang telah dilaksanakan dengan kaedah kekisi-Boltzmann (LBM) untuk aplikasi yang berkaitan dengan pengkapsulan isian bawah. Dalam kajian ini, LBM akan digunakan untuk mensimulasikan proses pengkapsulan untuk sendi pateri yang berlainan bentuk, penyusunan sendi pateri dan cara dispens. Sesetengah keputusan simulasi yang diperolehi dengan LBM akan dibandingkan dengan keputusan yang diperolehi daripada eksperimen pengimejan velocimetri partikel (PIV). Keputusan yang diperolehi daripada simulasi LBM dan eksperimen PIV adalah lebih kurang seiras. Dari segi penyusunan sendi pateri, adalah didapati bahawa penyusunan jajaran keliling memberikan masa pengisian yang paling singkat berbanding dengan penyusunan jajaran kosong tengah dan penuh. Bagi kaedah suntikan berbeza, adalah didapati bahawa kaedah penyutikan jenis U memberikan pengurangan masa pengisian sebanyak 67% berbanding dengan penyuntikan jenis I. Namun, ruang kosong yang besar dibentuk dengan kaedah suntikan jenis U. Suntikan jenis L pula menunjukkan pengurangan masa isian sebanyak 45% tanpa formasi ruang kosong makro. Di samping itu, kesan bentuk sendi pateri yang berbeza juga dikaji. Jajaran sendi pateri dengan sendi berbentuk jam pasir berjaya mengurangkan masa pengisian sebanyak 10% sambil menghasilkan ruang kosong yang lebih kecil. Sendi pateri berbentuk silinder tidak menunjukkan sebarang penambahbaikan yang ketara kepada masa pengisian kalau dibandingkan dengan pengisian bawah dengan sendi pateri

konvensional yang berbentuk sfera terpenggal. Isian bawah tekanan dapat mengurangkan masa pengisian sehingga 99% berbanding dengan isian bawah konvensional. Tekanan maksimum dalam domain aliran adalah lebih kurang 2.5 hingga 3 kali lebih tinggi daripada tekanan masuk semasa isian bawah yang disebabkan oleh pembinaan tekanan.

# **SIMULATION OF UNDERFILL ENCAPSULATION OF ELECTRONIC PACKAGING USING LATTICE-BOLTZMANN METHOD**

## **ABSTRACT**

Many finite volume method (FVM) based studies had been conducted by researchers to optimize and improve the underfill encapsulation process. However, there are limited studies conducted using lattice-Boltzmann method (LBM) for underfill encapsulation process. In this study, LBM will be used to simulate the encapsulation process of different solder joint shapes, different solder joint arrangements and injection methods. Some of the simulation results obtained using LBM will then be compared with the results obtained from experiment using particle image velocimetry (PIV) method. High conformity were obtained from both LBM and PIV results. In terms of the solder ball arrangements, perimeter arrangement was found to give the shortest filling time compared to middle empty and full arrangements. As for different injection methods, it was found that U-type injection gives a 67% reduction of filling time compared to I-type injection. However, a huge void is formed with U-type injection. Meanwhile, L-type injection shows a 45% reduction of filling time with no macro void formed. Furthermore, the effect of different solder joint shapes are also studied. Solder joint array with hourglass shape solder joints managed to reduce the underfill filling time by around 10% while yielding a smaller void. Cylindrical shape joints did not show any significant improvement on the filling time compared to that with truncated sphere shape joints. Pressurised underfill was found to reduce filling time by up to 99% compared to conventional underfill. The maximum pressure within the flow domain was found to be approximately 2.5 to 3 times higher than the inlet pressure during pressurised underfill due to pressure build-up.

# CHAPTER ONE

## INTRODUCTION

### 1.1 Introduction

The constant demand by consumers for better performing electronic devices in smaller footprints had led constant innovation by engineers to fulfil such demand. Thus, integrated circuit packages of compact size, high reliability and high performance are required to cope with such stringent requirements. Quality and reliability of the package pose as a concern as we continue the drive towards miniaturisation of integrated circuit package. This is where the study of electronic packaging comes into place.

Electronic packaging is an engineering discipline which sought to provide enclosure and protective features which can be built onto electronic products and components. During the service lifetime of an electronic product, they are constantly being exposed to various environmental factors like heat, humidity and vibrations. Exposure to such factors are detrimental, and could potentially lead to failure of such electronic devices. In order to ensure the longevity of an electronic devices, it is essential to protect the electronics from such constant exposure.

Electronic components can be classified into hierarchies based on its level of packaging level as shown in Figure 1.1. The first level packaging provides interconnection between the IC chips with the module. A second level packaging provides an interconnection between the first level electronic package to a PCB. Fulfilling such connection could be completed either with through hole technologies or surface mount technologies. The assembly could be coated with a polymer layer to

provide additional protection towards them. Third level packaging can be realized by interconnecting several of those second level packaging onto a motherboard. A fourth level packaging would have the motherboard, together with its interconnected second level packaging, being assembled into its fixture or casing such to become a final product like a computer or a CD player, which could be used by the end user.

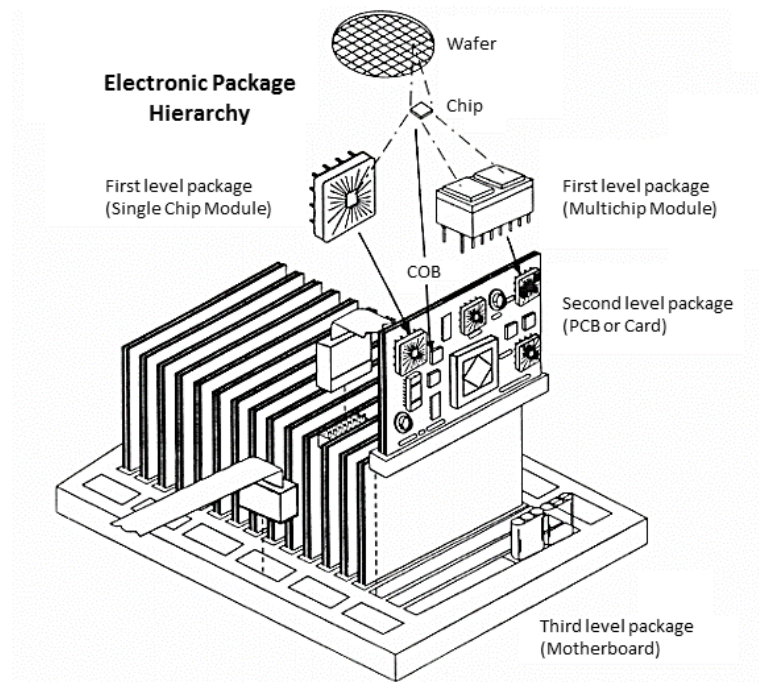


Figure 1.1: Electronic Packaging Hierarchy (Lau, 1994)

In this study, we are going to focus on the second level packaging, specifically, BGA encapsulation using underfill process. In SMT, small, intricate electronic components are mounted onto the surface of PCB without the need of through-hole mounting. BGA, being a type of SMT, utilizes small solder balls to form connection between the electronic components with the PCB. BGA outshines its SMT counterparts like pin grid array as it allows for higher interconnection density, better performance due to shorter leads, and better heat conduction. Figure 1.2 shows the arrangement of solder balls under an Intel Embedded Pentium MMX Processor.